Effective delivery of a microtubule polymerization inhibitor synergizes with standard regimens in models of pancreatic ductal adenocarcinoma

Jaime A. Eberle-Singh,[1,2] Irina Sagalovskiy,[1,2] H. Carlo Maurer,[1,2] Stephen A. Sastra,[1,2] Carmine F. Palermo,[1,2] Amanda R. Decker,[1,2] Min Jung Kim[3], Josephine Sheedy[3], Anna Mollin,[3] Liangxian Cao,[3] Jianhua Hu,[2,4] Arthur Branstrom,[3] Marla Weetall,[3] Kenneth P. Olive[1,2,4*]

[1] Division of Digestive and Liver Diseases, Department of Medicine, Columbia University Medical Center, New York, NY 10032
[2] Herbert Irving Comprehensive Cancer Center, Columbia University Medical Center, New York, NY 10032
[3] PTC Therapeutics, South Plainfield, NJ 07080
[4] Department of Biostatistics, Columbia University Medical Center, New York, NY 10032
[5] Department of Pathology & Cell Biology, Columbia University Medical Center, New York, NY 10032
* To whom correspondence should be addressed.

Running title: "Microtubule inhibition synergizes in pancreatic cancer"

Correspondence:
Kenneth P. Olive, Irving Cancer Research Center Room 217a, Columbia University Medical Center, New York, NY 10032. Phone: (212) 851-4678 Email: kenolive@columbia.edu

Disclosure of Potential Conflicts of Interest: Min Jung Kim, Josephine Sheedy, Anna Mollin, Liangxian Cao, Arthur Branstrom, and Marla Weetall are employees of PTC Therapeutics, which owns PTC596. The laboratory of Kenneth Olive received partial funding for this work (~15% of total) through a sponsored research agreement between Columbia University and PTC Therapeutics. No personal compensation or incentive was provided. Kenneth Olive is a member of the scientific advisory board of Elstar Therapeutics; there is no relationship between Elstar and the work presented in this manuscript.

Author Contributions: Conception and design: JAE, MW, AB, and KPO; experimental execution and acquisition of data: JAE, SAS, CFP, IS, MJK, JS, AM, LC, KPO; data analysis: JAE, KPO; computational biology analysis: HCM; statistical analysis: JAE, JH, KPO; writing, review and/or revision of text: JAE, KPO.

Transcriptomics data: Transcriptomic data generated in this work may be accessed via the GEO repository using the following confidential reviewer token:

ID: GSE118441

Token: krmbkmqebpajnuh

Statement of Translational Relevance

Pancreatic ductal adenocarcinoma (PDA) is responsible for more than 44,000 deaths per year in the United States. It is characterized by broad primary chemoresistance conferred in part by biophysical properties of the tumor stroma that interfere with drug delivery. Here we present and characterize PTC596, a novel microtubule polymerization inhibitor that demonstrates unusually promising pharmacological properties that bypass this barrier to drug delivery. Using multiple preclinical models, we demonstrate effective delivery of PTC596 to pancreatic tumor tissues, excellent tolerability, and significant preclinical efficacy in combination with standard therapies. In particular, PTC596 synergized potently with the nab-paclitaxel, a microtubule stabilizing agent used in combination with gemcitabine, providing strong evidence for combining these two distinct classes of microtubule targeted agents in patients with PDA.

Abstract

Purpose: Pancreatic ductal adenocarcinoma (PDA) is a deadly cancer that is broadly chemoresistant, due in part to biophysical properties of tumor stroma, which serves as a barrier to drug delivery for most classical chemotherapeutic drugs. The goal of this work is to evaluate the preclinical efficacy and mechanisms of PTC596, a novel agent with potent anticancer properties *in vitro* and desirable pharmacological properties *in vivo*.

Experimental Design: We assessed the pharmacology, mechanism, and preclinical efficacy of PTC596 in combination with standards of care, using multiple preclinical models of pancreatic ductal adenocarcinoma.

Results: We found that PTC596 has pharmacological properties that overcome the barrier to drug delivery in PDA, including a long circulating half-life, lack of P-glycoprotein substrate activity, and high systemic tolerability. We also found that PTC596 combined synergistically with standard clinical regimens to improve efficacy in multiple model systems, including the chemoresistant genetically engineered “KPC” model of PDA. Through mechanistic studies, we learned that PTC596 functions as a direct microtubule polymerization inhibitor, yet a prior clinical trial found that it lacks peripheral neurotoxicity, in contrast to other such agents. Strikingly, we found that PTC596 synergized with the standard clinical backbone regimen gemcitabine/nab-paclitaxel, yielding potent, durable regressions in a PDX model. Moreover, similar efficacy was achieved in combination with nab-paclitaxel alone, highlighting a specific synergistic interaction between two different microtubule targeted agents in the setting of pancreatic ductal adenocarcinoma.

Conclusions: These data demonstrate clear rationale for the development of PTC596 in combination with standard-of-care chemotherapy for PDA.

Keywords

pancreatic ductal adenocarcinoma; translational therapeutics; microtubule polymerization inhibitor; preclinical combinations

Introduction

An estimated 56,770 Americans will be diagnosed with pancreatic cancer in 2019 and this figure is predicted to rise over the next decade[1, 2]. Pancreatic ductal adenocarcinoma accounts for ~93% of pancreatic tumors but, despite some measurable progress in recent years, it remains a largely intractable cancer, with a five-year survival rate of 8.7%[3]. Among the most remarkable features of PDA is its broad primary resistance to chemotherapy, which is conferred at least in part by properties of the tumor stroma that limit drug delivery[4, 5]. We previously elucidated this concept using the *Kras*$^{LSL.G12D/+}$; *p53*$^{LSL.R172H/+}$; *PdxCre*$^{tg/+}$ (KPC) mouse[6], a well-validated genetically engineered model of PDA that recapitulates many of the features of human pancreatic cancer, including stromal desmoplasia and chemoresistance[4]. Thus, the KPC mouse serves as a highly stringent system in which to test the preclinical efficacy of novel agents for PDA.

Based on our earlier findings, we proposed that drug development efforts for PDA should focus on agents with a long half-life and a large therapeutic index (the range of concentrations between efficacy and toxicity) as a means of improving drug exposure[4]. Unfortunately, most traditional cytotoxic agents are rapidly cleared from circulation, are acutely toxic to normal proliferating tissues, are quickly metabolized, or are actively exported from tumor cells. An informative counterexample is nab-paclitaxel (Abraxane, Celgene), an albumin-bound form of the microtubule stabilizing agent paclitaxel that is FDA approved in combination with gemcitabine (a deoxycytidine analog) for metastatic PDA patients[7]. Nab-paclitaxel has a terminal half-life of 27 hours in circulation and is less toxic than unmodified paclitaxel[8]. The clinical success of the gemcitabine/nab-paclitaxel combination (which now serves as a standard backbone regimen for new clinical trials) helped to demonstrate the importance of pharmacology in pancreatic cancer drug development.

In the course of our work, we evaluated PTC596 (PTC Therapeutics, **Supplemental Figure 1**), a small molecule anticancer agent originally identified for its selective activity in cell lines with high levels of BMI1 protein[9]. We found that PTC596 potently induces mitotic arrest and apoptosis in multiple PDA cell lines. More unusual, we found that PTC596 has attractive pharmacological properties, including a long circulating half-life, lack of P-glycoprotein (P-gp) substrate activity, and effective biodistribution into autochthonous pancreatic tumors. Through a combination of transcriptomic, cellular, and biochemical studies, we determined that the mechanism of action of PTC596 is through direct inhibition of tubulin polymerization, although, in contradistinction to other microtubule targeted agents (MTAs), PTC596 is very well tolerated

in vivo. Critically, intervention studies in multiple preclinical models, including the genetically engineered KPC model, a cell line-based xenograft, and a patient-derived xenograft, demonstrated potent activity of PTC596 in combination with common backbone regimens for PDA. In particular, combining PTC596 with gemcitabine/nab-paclitaxel, or even just with nab-paclitaxel alone, produced frank, durable regressions in a patient-derived xenograft model of PDA, revealing a synergistic interaction between two distinct microtubule-targeted agents, each possessing strong pharmacological properties.

Methods

Additional details are presented in Supplementary Materials for all experiments.

Animal Studies: All animal studies were carried out in accordance with approved Institutional Care and Use Committee protocols for Columbia University Medical Center (AC-AAAQ-1415), PTC Therapeutics, or Champions Oncology (PDX Model).

Cell lines, cell culture, and viability assays

Authenticated human cell lines were purchased from ATCC, utilized within 30 cumulative passages of initial purchase. Murine KPC lines were generated previously by KPO and used within 30 cumulative passages. J1002 cells were generated by JAE from KPFBR mice and used within 15 cumulative passages. All cell lines consistently tested negative for mycoplasma throughout the period of experimentation using the MycoAlert Mycoplasma Detection Kit (Lonza). Cells were cultured in DMEM + 10% FBS with pen/strep. Proliferation and dose response curves were performed in 96 well plates, with viability measured by AlamarBlue (BioRad) according to standard protocols. All assays were carried out in at least triplicate with 4-8 technical replicates per treatment group, per experiment. Colony formation assays were performed according to standard protocols, with 3000 cells per 6-well for murine cells and 5000 cells per 6-well for human cells, in triplicate.

Flow cytometry

For cell cycle analysis, log-growth phase cells were treated with agents as indicated, harvested, fixed in cold 70% ethanol, resuspended in PBS + 2% FBS + 3μM DAPI or 0.25ug 7-AAD, and analyzed using a MACSQuant Analyzer 10 (Miltenyi) or BD LSRII. Data were analyzed using FlowJo software. For intracellular proteins, experimental conditions were

similar, but cells were fixed/permeabilized using the eBioscience Foxp3/Transcription Factor Staining Buffer Set (ThermoFisher, 00-5523-00), blocked with Fc Block (BD Biosciences, 564220) and stained with anti-PH3 (BioLegend, 650805), analyzed on a BD Fortessa, and analyzed by FlowJo. Active Caspase-3, was performed according to manufacturer's instructions (Abcam, ab65613).

Western blotting

Western blotting was performed according to standard procedures using the following antibodies: Bmi1,Cell Signaling #5856, 1:1000; Vinculin, Cell Signaling #4650S, 1:1000; Beta-tubulin, Cell Signaling #2146S, 1:1000; Anti-rabbit IgG, HRP-linked Antibody, Cell Signaling, #7074, 1:5000.

P-glycoprotein substrate activity experiment

MDCKII-mdr1 and MDCKII-wt cells were purchased from the Netherlands Cancer Institute, NKI-AVL. Cells were cultivated in DMEM + FBS + 1% Penn/Strep, and used between passage 3-9. Cells were plated for 4 hours, treated as indicated, and viability measured using Cell Titre-Glo (Promega).

RNA sequencing

Illumina Tur-Seq RNA libraries were prepared from poly-A enriched mRNA and sequenced on an Illumina HiSeq 4000 to 30 million 100bp single reads. Reads were mapped to (NCBI/build 37.2) using the STAR aligner (version 2.4.2)[10] and were quantified at the gene level using the *summarizeOverlaps* function from the R package 'GenomicAlignments'[11] with information on gene annotations from the R package 'TxDb.Hsapiens.UCSC.hg19.knownGene'.[12] RNA-seq data were deposited to GEO (ID: GSE118441).

Expression analysis

Differential gene expression was performed using the *voom-limma* framework.[13] Single sample GSEA: gene set variation analysis was performed in R according to default parameters.[14]

Cell-free tubulin polymerization assay

Assay was performed using the fluorescence-based tubulin polymerization assay kit from Cytoskeleton (#BK011P), according to instructions. Polymerization rates (fluorescence units/minute) were determined by measuring the maximal slope (by linear regression) of the linear portion of the growth phase of the polymerization curve.

Analysis of free tubulin content

Free vs. polymerized tubulin was measured using the Microtubule/Tubulin In Vivo Assay Biochem Kit (Cytoskeleton, #BK038).

Immunocytochemistry

Cells were seeded onto acid-washed, poly-L-lysine coated glass coverslips in 12-well plates. At mid-confluency, cells were then treated as indicated for 24 hours, washed with TBS, and extracted with Brinkley Buffer 1980 for 30 seconds. Cells were fixed for 20 minutes in 4% formaldehyde, 10 mM MES pH 6.1, 138 mM KCl, 3 mM $MgCl_2$, 2 mM EGTA, 0.32M sucrose. Following fixation, cells were washed with TBS and then blocked in TBS-T (0.1% Triton-X) + 2% BSA + 22.52 mg/mL glycine for 30 minutes, followed by an overnight incubation in primary antibody (Abcam179513, 1:1000) at 4°C and then secondary antibody for one hour at room temperature (Life Technologies, A11012, 1:500). Cells were counterstained with DAPI before mounting. Confocal imaging was performed using an A1 laser scanning confocal attachment on an Eclipse Ti microscope stand using a 60x/1.49 ApoTIRF oil-immersion objective and standard lasers and filter sets (Nikon Instruments, Melville, NY).

Animal breeding and genotyping

Genetically engineered models were generated by intercrossing strains as listed in Supplementary Methods, with genotyping performed by Transnetyx (Cordova, TN). Strains were of mixed genetic background. Studies utilized both male and female animals. Animals were provided standard chow and housed under a 12-hour light/dark cycle.

Capan1 Xenograft Intervention Study

7-week old NCr *nu/nu* athymic nude mice were inoculated subcutaneously with $5x10^6$ Capan-1 cells suspended in matrigel (N= 10/group). When the mean tumor volume was ~212 mm^3, mice were randomized to treatment with: vehicle, PTC596 (12.5mg/kg, b.i.w., p.o.), gemcitabine (100mg/kg, b.i.w., i.p.), or full dose combination of PTC596 + gemcitabine. At Day 45, dosing

was stopped. Length (L) and width (W) diameters of tumors were measured using digital calipers and mice were weighed twice per week. Tumor volume was calculated as (L X W^2)/2.

PDX Model Intervention Study

Study was performed by Champions Oncology. Early passage tumor fragments from Champions model CTG-1462 were implanted subcutaneously in *nu/nu* mice and then randomized to a treatment arm once tumors reached 150 – 300mm^3. Mice (n= 5/group) were treated on one of seven arms: vehicle, gemcitabine (50mg/kg, q.w., i.p.), nab-paclitaxel (10mg/kg, i.v., q.w.x3), PTC596 (12.5mg/kg, b.i.w.x4, p.o.), or full dose combinations of the agents. Endpoints were when a tumor reached 1500mm^3 or after 90 days on study. Length (L) and width (W) diameters of tumors were measured using digital calipers and mice were weighed twice per week. Tumor volume was calculated as (L x W^2)/2.

KPC Intervention/Survival Study

Tumor formation in KPC mice was monitored by weekly palpation until the detection of a mass. Upon positive palpation, the mass was monitored by twice weekly ultrasound[15] until the tumor reached an enrollment size of 4-7 mm average diameter. Following enrollment, KPC mice were randomized to vehicle, PTC596 (17 mg/kg, PO, b.i.w.), gemcitabine alone (100 mg/kg, IP, b.i.w.), or PTC596 + gemcitabine.

Measurement of PTC596 levels in plasma and tissue samples

Concentrations of PTC596 in samples were quantified using high-performance liquid chromatography with tandem mass spectrometry (LC-MS/MS).

Survival data synergy analysis

To test for synergy between gemcitabine and 596 treatments in the KPC intervention study, we generated a regression model for logarithm-transformed survival times from mice treated with vehicle, gemcitabine, PTC596, and an interaction term for gemcitabine + PTC596. The significance of the gemcitabine:PTC596 interaction term tests the single-tailed deviation of the combination arm from the additive effects of each agent alone.

Immunohistochemistry

Immunohistochemistry (IHC) was performed according to standard protocols. Slides were blocked for one hour at room temperature in TBS-T (0.1% Tween20) + 1.5% normal horse

serum (Vector Laboratories, S-2000) + 2% Animal Free Blocker (Vector Laboratories, SP-5030). Primary antibodies were diluted in blocking solution and incubated overnight at 4ºC at the indicated concentrations and then developed using the ImmPRESS and ImmPACT kits (Vector). PH3: Cell Signaling, #9701, 1:100; CC3: Cell Signaling, #9664S, 1:100.

Results

PTC596 induces mitotic arrest and apoptosis in PDA cell lines

Based on our initial interest in the potential role of BMI1 in pancreatic cancer[16], we assessed the effects of PTC596 on the viability of PDA cell lines. We treated three human PDA lines (Aspc1, Mia PaCa-2, and Panc1) with PTC596 or vehicle and found that the agent potently reduced cell viability over the course of 96 hours in all cell lines (**Figure 1A, Supplemental Figure 2A**). The cytotoxicity of PTC596 was confirmed in colony formation assays on the same lines (**Supplemental Figure 2B**). Next we performed cell cycle analysis using intracellular 7-AAD staining and found that PTC596 induced a G_2/M arrest, similar to the anti-mitotic agent nocodazole (**Figure 1B,C; Supplemental Figure 2C**). Flow cytometry for the M-phase marker phospho-histone H3 (PH3) demonstrated an accumulation of PDA cells specifically in mitosis following PTC596 treatment (**Figure 1D,E; Supplemental Figure 2D**). These data demonstrate that PTC596 acts as a potent inducer of mitotic arrest in multiple PDA cell lines.

The mitotic checkpoint exists to ensure that chromosomes are appropriately attached to microtubules prior to cell division[17]. If the triggering stress is not resolved, prolonged mitotic arrest may result in apoptosis or, alternatively, progression into a pseudo-G_1 phase in the absence of cytokinesis. Particularly, in the context of *p53* mutations, this can lead to cell cycle re-entry and eventual polyploidization through the process of endoreduplication[18, 19]. As *p53* is mutated in ~78% of human ductal adenocarcinomas[20], we examined DNA content in three *p53* mutant human PDA lines following treatment with PTC596. Over the course of 72 hours, we observed a progressive increase in DNA content, eventually leading to >60% of cells bearing >4N DNA content (**Figure 1F,G; Supplemental Figure 3A,B**). This was accompanied by increased levels of apoptosis that progressively increased over the same timeframe in all three lines, as measured by the caspase-activated probe FITC-DEVD-FMK (**Figure 1H,I**). Thus, PTC596 induces responses in pancreatic tumor cell lines consistent with prolonged mitotic checkpoint activation, including polyploidization and cell death.

PTC596 has favorable pharmacological properties

Many candidate anticancer agents demonstrate promising activity *in vitro*, but are either too toxic or have poor pharmacological properties when administered *in vivo* – problems that are compounded by the characteristic hypoperfusion of ductal pancreatic tumors[4]. Prior work in xenograft models of acute myeloid leukemia (AML) suggested that PTC596 is generally well tolerated[21], but its delivery to solid tumor tissues has not been assessed. In anticipation of studies in the KPC model, we treated five PC mice per timepoint ($p53^{LSL.R172H/+}$; $Pdx1Cre^{tg/+}$ – KPC littermates that are phenotypically normal) with a single oral dose of 10 mg/kg PTC596 and examined circulating drug levels over a period of 48 hours (**Figure 2A**). After 7 hours, plasma concentrations of PTC596 peaked at 8.9 μg/mL and then diminished over the course of two days, yielding a terminal half-life of ~15 hours, which compares favorably with the pharmacokinetics of other traditional cytotoxic agents. Thus, PTC596 persists in circulation for sufficient time to potentially equilibrate within poorly perfused pancreatic tumors.

In addition to imposing biophysical constraints on drug delivery, tumor cells can actively pump out many chemotherapeutic drugs via the multidrug transporter P-glycoprotein (P-gp). We examined the impact of P-gp expression and inhibition on drug sensitivity by using a congenic pair of cell lines (MDCK-WT and MDCK-PGP) with or without overexpression of human *ABCB1* (the gene encoding P-gp) and co-treating with treating the P-gp inhibitor Valspodar. We measured the viability of these cell lines over 72 hours in response to increasing concentrations of PTC596 or other agents, in the presence or absence of Valspodar (**Figure 2B,C**). For several chemotherapeutic agents known to be P-gp substrates, including vinblastine and paclitaxel, overexpression of P-gp increased the CC_{50} by 10 – 30 fold, an effect that was fully reversed by co-treatment with Valspodar. By contrast, both PTC596 and its analog PTC028[22] were fully unaffected by P-gp overexpression or inhibition, indicating that these agents are not susceptible to this multi-drug resistance mechanism.

To directly assess the delivery and accumulation of PTC596 to pancreatic tumor tissues, we performed a short-term study in pancreatic tumor-bearing KPC mice following administration of a single dose of 17 mg/kg PTC596. After 24 hours, tissues were harvested, frozen, extracted, and analyzed by mass spectrometry (**Figure 2D**). Prior studies have shown that pancreatic tumor stroma limits the accumulation of other chemotherapeutic agents relative to normal tissues[4, 23]. In contradistinction, PTC596 was effectively delivered to pancreatic tumor tissues, achieving levels comparable to those observed in quadriceps muscle, spleen, and brain tissues.

Higher levels were detected in liver and kidney tissues, the primary routes of clearance for PTC596. We next examined whether co-treatment with gemcitabine altered the delivery of PTC596 to tissues, using a similar study design in the related KP$^{fl/fl}$C (Kras$^{LSL.G12D}$/+; p53$^{fl/fl}$; Pdx1-Cre$^{tg/+}$) model, and found no effect of gemcitabine on the pharmacology of PTC596 (**Figure 2E**). Together these data demonstrate that PTC596 can be effectively distributed into PDA tissues, alone and in combination with gemcitabine, despite the unique biophysical constraints on drug delivery to pancreatic tumors.

Having established the effective delivery of PTC596 to tumor tissues, we next examined the pharmacodynamic response of murine pancreatic tumors to PTC596. We began by confirming that PDA cells derived from the KPC model behave similarly to human PDA cells in response to treatment with PTC596 (**Supplemental Figure 4**). We then evaluated the impact of PTC596 on mitotic arrest *in vivo* by measuring expression of the mitotic protein Cyclin B1 in tumors from KP$^{fl/fl}$C mice. We performed a second short-term intervention study in tumor-bearing KP$^{fl/fl}$C mice (n= 3), this time acquiring a pre-treatment biopsy by abdominal laparotomy[24] and then treating with 10 mg/kg PTC596 on days 0, 2, 4. On day 5, the mice were euthanized and tissues harvested, 24 hours after the final dose (**Supplemental Figure 5A**). Western blotting for Cyclin B1 was performed on lysates from paired pre- and post-treated tumor samples (**Figure 2F**). Cyclin B1 protein levels were significantly increased in post-treatment samples relative to pre-treatment samples, indicating that the delivery of PTC596 to tumor tissues was sufficient to induce a pharmacodynamic response *in vivo*.

Finally, we assessed the tolerability of prolonged treatment with PTC596 in combination with gemcitabine, using KC mice (*Kras$^{LSL.G12D/+}$; Pdx1-Cre$^{tg/+}$*) as surrogates for the KPC model. We found that these mice tolerated up to 17 mg/kg PTC596 (p.o., q.w.) in combination with 100 mg/kg gemcitabine (i.p., b.i.w) for at least one month (**Figure 2G**). Together, these data demonstrate that PTC596 is a well-tolerated agent with a prolonged half-life and effective biodistribution that induces an acute pharmacodynamic response in pancreatic tumor tissues.

PTC596 + gemcitabine exhibit activity in preclinical models of pancreatic cancer

To begin to assess the preclinical efficacy of PTC596, we generated cell-line based xenografts from Capan-1 human PDA cells implanted subcutaneously in nu/nu mice. One week after implantation, when the implanted tumors had reached ~200 mm^3, mice were randomized

to one of four treatment arms: vehicle, PTC596 alone at a sub-maximal dose for this strain (12.5mg/kg, b.i.w., p.o.), gemcitabine (40mg/kg, b.i.w., i.p.), or both agents combined (N=10/group). Over the course of 45 days, we found that PTC596 slowed tumor growth modestly as a monotherapy **(Figure 3A)**, and induced transient regressions in combination with gemcitabine. Both regimens were well tolerated as evidenced by longitudinal weight measurements **(Figure 3B)**.

Next, in order to evaluate the activity of PTC596 in a more physiologically accurate model, we carried out an intervention/survival study in the KPC genetically engineered mouse model. Nascent autochthonous pancreatic tumors were identified and measured by high resolution 3D ultrasound[15] and the volume of each tumor was tracked longitudinally during treatment (**Supplemental Figure 5B**). Mice were randomized to one of four treatment arms: vehicle, PTC596 alone (17 mg/kg, b.i.w., p.o.), gemcitabine (100 mg/kg, b.i.w., i.p.), or PTC596 + gemcitabine (full-dose combination); this regimen was well-tolerated in tumor-bearing KPC mice (**Figure 3C**). Strikingly, while neither PTC596 nor gemcitabine alone impacted survival, we found that the two agents synergistically increased overall survival by more than 3-fold over vehicle-treated animals ($p= 0.033$ for interaction term of a Cox proportional hazards model) (**Figure 3D**). Using longitudinal 3D ultrasound data, we reconstructed growth curves for each tumor over time and found that while PTC596 + gemcitabine did not induce tumor regressions, the combination durably reduced tumor growth rate (**Supplemental Figure 5C,D**). Using a published algorithm[25], we modeled the growth/decay kinetics of each tumor and found that PTC596 reduced tumor growth rate both in combination with gemcitabine, and also as a monotherapy (**Figure 3E; Supplementary Figure 5E**). Examination of liver sections revealed no significant difference in the fraction of animals free of metastasis following treatment (**Supplemental Figure 5F**).

We next assessed whether PTC596 induced mitotic arrest in the KPC tumors using immunohistochemistry (IHC) for phospho-Histone H3 (PH3). We found that PH3 was significantly elevated in the PTC596 monotherapy group compared to vehicle **(Figure 3F)**, consistent with an increased mitotic fraction (**Supplemental Figure 6A-D**). A trend towards increased PH3 staining was also observed in the combination treated mice; we speculate that the induction of G_1 arrest by gemcitabine reduces the fraction of cells arrested in mitosis, consistent with the overall lower growth rate of tumors treated with PTC596 + gemcitabine.

Finally, we performed IHC for the apoptotic marker cleaved Caspase-3 (CC3) on the same endpoint tumor samples. While none of the treatments significantly elevated the overall fraction of CC3 positive cells, (**Figure 3G**), half of the tumors in the PTC596/gem group exhibited elevated levels of apoptosis relative to vehicle-treated tumors (**Supplemental Figure 6E,F**). This finding is notable given that the samples were collected at endpoint when the tumors have largely escaped the initial effects of drug treatment. Together, these findings demonstrate that PTC596 can contribute to an effective anticancer response in models of PDA, particularly as part of a combination regimen with a standard of care agent.

PTC596 functions independent of *Bmi1* in PDA cells

PTC596 was previously reported to be a BMI1 inhibitor[21]. However, the induction of mitotic arrest by PTC596 in multiple cell lines (**Figure 1**) contrasts with the findings of several prior studies in which silencing of *Bmi1* with shRNAs or miRNAs was shown to induce a G_1 arrest[26-30]. In both human PDA and AML[21] cell lines, PTC596 treatment was associated with hyperphosphorylation of BMI1 (**Figure 4A,B**), suggesting the possibility that modulation of BMI1 is a component of the mechanism of action of PTC596. Incidentally, we noted that nocodazole, a chemical that induces mitotic arrest through inhibition of tubulin polymerization, also induces BMI1 hyperphosphorylation (**Figure 4A**). Indeed, BMI1 was previously reported to be phosphorylated and dissociated from chromatin during mitosis, indicating that BMI1 phosphorylation is cell cycle dependent[31]. Thus, PTC596 may impact BMI1 as an indirect consequence of inducing mitotic arrest; however, the functional role of BMI1 in the activity of PTC596 is uncertain.

To directly assess the role of Bmi1 in PTC596 activity, we used a dual recombinase strategy to generate *Kras*$^{FSF.G12D}$/+; *Tp53*$^{R172H/+}$; *Pdx1-FlpO*$^{tg/+}$; *Bmi1*$^{fl/fl}$; *Rosa26*$^{CreERT2/+}$ (KPFBR) mice, in which the *Bmi1* gene can be acutely deleted in the context of *Kras/p53* mutant pancreatic tumors (see Methods). We derived a PDA cell line (J1002) from an autochthonous pancreatic tumor arising in a KPFBR mouse, and treated it *in vitro* with 4-hydroxy-tamoxifen or vehicle, yielding congenic lines that were wild-type (J1002VEH) or null (J1002TAM) for *Bmi1* (**Figure 4C,D**). We then treated each line with PTC596 and examined cell viability over the course of 96 hours. Notably, *Bmi1* deletion in J1002 cells did not impact the ability of PTC596 to inhibit cell proliferation (**Figure 4E,F**) or induce mitotic arrest (**Figure 4G,H**). These studies

indicate that the antiproliferative effects of PTC596 in pancreatic tumor cells are not dependent on the function of BMI1.

PTC596 inhibits microtubule polymerization

In order to learn more about the impact of PTC596 on PDA cells, we performed RNA sequencing on Aspc1 cells treated with either DMSO or 1.0 μM PTC596 for 8, 16, and 24 hours. Integrating the data from experimental and control samples across all three timepoints, we found that genes differentially expressed between PTC596 vs. DMSO treated cells were strongly enriched in mitotic processes and depleted in processes associated with S-phase or the G_1/S transition (**Supplemental Figure 7A**). Moreover, PTC596 treatment led to significant down-regulation of multiple α- and β-tubulin genes (**Figure 5A**). Indeed, tubulin genes accounted for eight out of ten of the most down-regulated genes in response to PTC596 treatment. Tubulin gene transcripts are subject to tight autoregulation based on the abundance of free tubulin monomer, which increases following inhibition of tubulin polymerization[32]. These findings led us to hypothesize that PTC596 might function as a microtubule polymerization inhibitor.

We first tested this hypothesis through ultracentrifugation of protein lysates from vehicle or PTC596-treated Aspc-1, Mia PaCa-2, and Panc1 cells. In this assay, large polymerized microtubules pellet at low speeds (5,000 x g) whereas free tubulin monomers remain in the supernatant even following high-speed ultracentrifugation (100,000 x g). Visualization of tubulin fractions by western blotting demonstrated that PTC596 treatment led to a near-complete loss of polymerized microtubules, similar to the effects of colchicine, a well-known microtubule polymerization inhibitor **(Figure 5B; Supplemental Figure 7B)**. Consistent with this finding, we observed a striking loss of polymerized microtubules in three different human PDA lines following PTC596 treatment, as visualized by β-tubulin immunofluorescence, with the few remaining microtubules assuming an altered, irregular pattern (**Figure 5C,D; Supplemental Figure 7C**).

Microtubule polymerization is facilitated and regulated by numerous cellular proteins[33]. In order to determine whether PTC596 directly affects microtubule polymerization, we carried out a biochemical polymerization assay using >99% purified tubulin and GTP in a reaction buffer. We assessed the impact of PTC596 in this cell-free assay at multiple concentrations. Notably, we

found that PTC596 inhibited tubulin polymerization in a dose-dependent manner, similar to colchicine, whereas paclitaxel, a microtubule stabilizing agent, accelerated polymerization kinetics **(Figure 5E,F)**. These findings demonstrate that PTC596 functions as a direct inhibitor of microtubule polymerization.

The preclinical efficacy of PTC596 in PDA is synergistic with gemcitabine/nab-paclitaxel

PTC596 and nab-paclitaxel appear to share several similarities. Both are microtubule targeted agents with attractive pharmacological properties and both combine effectively with gemcitabine in the treatment of PDA, at least in a preclinical setting. However, nab-paclitaxel is already clinically approved in combination with gemcitabine for the treatment of metastatic PDA, and now serves as a prominent backbone regimen for clinical trials of new investigational agents. Given this clinical landscape, is there a rationale for adding a microtubule polymerization inhibitor to a regimen that already includes a microtubule stabilizing agent?

Combinations of multiple microtubule targeted agents have been explored clinically in several cancers, particularly in breast cancer where the combination of vinorelbine + paclitaxel was found to be tolerable and have promising efficacy in Phase II trial of second-line patients with advanced disease[34]. However, multi-MTA regimens have not been explored in the context of pancreatic ductal adenocarcinoma. We therefore carried out a 7-arm intervention study using a PDA patient-derived xenograft model, evaluating all combinations of gemcitabine, nab-paclitaxel, and PTC596 (n= 5 per arm). As expected, pairing gemcitabine with nab-paclitaxel slowed tumor growth to a greater degree than either agent alone (**Figure 5G**), and this was reflected in growth constants derived from their respective tumor volume curves (**Supplemental Figure 7D**). In this model, PTC596 exhibited similar anticancer activity to nab-paclitaxel, both as a monotherapy and in combination with gemcitabine. Strikingly, the triple combination of gemcitabine/nab-paclitaxel/gemcitabine had a remarkable effect on the viability of this PDX model, producing sizeable and durable regressions in all five animals evaluated, including one complete response (**Supplementary Figure 7E,F**). The induction of tumor regressions was evident in our modeling of tumor volume kinetics, which produced a decay term for all five animals, three of which had no associated growth term. Moreover, the increased efficacy of this regimen was achieved without a measurable impact on tolerability, as evidenced by longitudinal weight measurements (**Figure 5H**). Unexpectedly, we noted that the two–drug combination of nab-paclitaxel + PTC596 was nearly as active as the three–drug combination, yielding

regressions in four of five tumors. Thus, rather than functioning through redundant mechanisms, we found that the combination of a microtubule polymerization inhibitor with a microtubule stabilizer yielded a potent synergistic effect on preclinical efficacy in pancreatic ductal adenocarcinoma without appreciable effects on tolerability.

Discussion

Over the course of 65 years, microtubule targeted agents have been the most successful class of anticancer agents, with approved applications in leukemia, lymphoma, breast, non-small cell lung, and pancreatic cancers, among others. First approved by the FDA in 1962[35], vincristine (Oncovin) was initially isolated from the periwinkle plant (*Catharanthus roseus*) and determined to be myeloablative, with anticancer activity in models of lymphocytic leukemia[36]. Over the subsequent decades, more than half a dozen additional MTAs received FDA approval, mostly for oncology applications. Different subclasses of these agents are distinguished by their binding sites on tubulin, which determines their ability to inhibit or stabilize microtubule polymerization. However, as a class, MTAs have been limited by broad toxicities, poor pharmacological properties, and an overly simplistic understanding of the cellular mechanism(s) through which they induce antineoplastic activity. In the past few decades, two major advances were made with the FDA approvals of eribulin (Halavan) and nab-paclitaxel (Abraxane), with each proving informative as to how further advances may be realized.

Prior to the development of eribulin, all clinical MTAs bound to one of three sites on tubulin: the vinca and colchicine sites for inhibitors of microtubule polymerization and the taxane site for microtubule stabilizers. By contrast, eribulin inhibits microtubule polymerization through non-competitive binding to another site, resulting in the formation of small globular aggregates of tubulin (rather than releasing free tubulin, like prior polymerization inhibitors)[37]. This subtle mechanistic difference is associated with reduced toxicity relative to vinca agents and has led to approvals in metastatic breast cancer and liposarcoma[38]. Given that colchicine, eribulin, vinca agents, and taxanes all effectively reduce the normal function of tubulin and induce mitotic arrest, why might their activity and toxicity profiles vary so broadly?

As microtubules play a critical role in the separation of chromosomes during mitosis, resulting in mitotic arrest, it was long assumed that the primary antineoplastic mechanism of MTAs was through mitotic checkpoint activation. Based on this logic, inhibitors of several mitotic

checkpoint proteins, including aurora kinases, polo-like kinases, and kinesin spindle protein, were developed[39-41]. However, across 46 clinical trials for 20 mitosis–specific inhibitors, the overall response rate was just 1.6%[42]. Therefore, the most relevant antineoplastic effects of MTAs may in fact be their impact on other microtubule associated processes. Indeed, one of the main side effects of MTAs as a class is neurotoxicity, which is mediated by effects on post-mitotic neurons. Microtubule dynamics play critical roles in the functioning of heat shock proteins, endosomal trafficking, cell migration, and other key aspects of cell biology[43-45]. Similarly, some MTAs induce vascular remodeling in addition to tumor cell apoptosis, through uncertain mechanisms[46, 47]. These cellular functions are mediated by distinct pools of microtubules with different biochemical properties conferred by interactions with varying sets of microtubule associated proteins. Thus, subtle differences in the binding of an MTA to tubulin will likely have diverse impacts on various cellular functions.

The second recently–approved MTA was nab-paclitaxel, a reformulated variant of the microtubule stabilizing agent paclitaxel. The key advance of nab-paclitaxel is its improved pharmacology over native paclitaxel, which is poorly soluble and rapidly cleared from circulation. A carrier agent, cremophor, is utilized for solubilization of paclitaxel in the clinical formulation, but cremophor itself confers significant additional toxicity. In nab-paclitaxel, the parent drug is stabilized by binding to albumin, increasing its solubility while lowering toxicity and maintaining prolonged stability in circulation. Given that drug delivery is compromised in pancreatic ductal adenocarcinoma due to poor perfusion and diffusion within the tumor parenchyma[4], prolonged circulation and low toxicity are desirable features for novel agents against this disease. Indeed, in 2015, a positive Phase III trial of nab-paclitaxel in combination with gemcitabine led to its approval for use in metastatic pancreatic cancer[7].

Together these examples proffer a compelling case that novel microtubule targeted agents have the potential to play an important role in the future of oncology, particularly those with novel biochemistry, attractive pharmacology, and low toxicity. PTC596 provides a strong example of such an agent, with a long circulating half-life and evidence of the accumulation of efficacious concentrations of the agent in genetically engineered pancreatic tumors. It is worth noting that tubulin is among the most abundant proteins in a proliferating cell, and thus may act as a sink for the stabilization and retention of tubulin-binding drugs. Combined with the lack of drug efflux via P-glycoprotein, these features may serve to elevate intratumoral concentrations while limiting peripheral toxicity. Indeed, in a multi-center Phase I study in advanced solid tumors (NCT02404480), PTC596 was generally well tolerated through six dose levels and target

plasma concentrations were achieved well below the highest dose[48]. Primary side effects were manageable and generally gastrointestinal in nature. Critically, no evidence of peripheral neuropathy was observed, distinguishing PTC596 from nearly all other microtubule targeted agents. A Phase 1b study in combination with paclitaxel and carboplatin for patients with advanced ovarian cancer (NCT03206645) is ongoing.

Both in ovarian cancer and in PDA, current backbone regimens include taxanes, raising the question of whether adding a microtubule polymerization inhibitor is likely to confer additional benefit. The principle rationale for combining such agents is that they may each impact different subsets of microtubule functions in different ways. Preclinical synergy between vinca agents and taxanes has been reported both *in vitro*[49, 50] and *in vivo*[51] and multiple early phase clinical trials have been performed in breast, non-small cell lung, and other cancers[34]. For example, in a clinical study of paclitaxel and vinorelbine in metastatic breast cancer, 6 complete responses and 19 partial responses were observed among 52 patients. While main toxicities were neutropenia and neurotoxicity, they were reported to be mild and well tolerated[52]. Thus, there is both rationale and precedent for combining microtubule polymerization inhibitors and stabilizers in an oncology setting. In that context, the observation of durable regressions in a pancreatic cancer PDX model exclusively among tumors treated with both nab-paclitaxel and PTC596 is a highly promising signal of preclinical efficacy. Ideally, this combination would have also been evaluated in an autochthonous model system such as KPC mice; however, the human albumin component of nab-paclitaxel induces anaphylaxis in immune-competent animals after prolonged exposure[53, 54]. Nonetheless, even the two-drug combination of PTC596 + gemcitabine produced a 3-fold extension of overall survival in the KPC model, matching or exceeding the best responses reported to date for this highly chemoresistant model. Taken together, we believe these data provide strong rationale for the clinical development of PTC596 combination strategies in the context of pancreatic ductal adenocarcinoma.

Acknowledgements

KPO received support for this work from the National Cancer Institute (1R21CA188857), the Stewart Trust Cancer Research Fellowship, and sponsored research support from PTC Therapeutics. JAE received support from an NIH training grant (5T32CA009503). The *Bmi1*^{flox} allele was generously provided by the laboratory of Dr. Marina Pasca di Magliano, with permission from Dr. Sean Morrison, who generated the allele. The Pdx-FlpO allele was kindly

provided by E. Scott Seeley. The work made use of several shared resources of the Herbert Irving Comprehensive Cancer Center (P30CA013696) including: Confocal and Specialized Microscopy, Flow Cytometry, Small Animal Imaging, and Molecular Pathology.

Figure 1 – PTC596 inhibits proliferation of PDA cell lines by inducing G2/M arrest, polyploidy, and ultimately cell death. **(A)** Relative Aspc1 cell viability over 96 hours following treatment with vehicle or indicated concentrations of PTC596. Asterisks indicate significance at final timepoint. **(B)** Representative histograms of DNA content, measured by flow cytometry for 7-AAD fluorescence, from Aspc1 cells treated for 24 hours with vehicle or PTC596. **(C)** Percent of Aspc1 cells in G0/G1 phase, S phase, and G2/M phase following 24 hours treatment with vehicle (DMSO), PTC596 (0.1 uM, 1.0 uM), 0.1 uM nocodazole (NOC, positive control). Chi^2 test with multiple hypothesis correction for indicated comparisons, with p-values integrated across the three experiments by Stouffer's method. (**D)** Representative flow cytometry scatter plots of phosphorylated histone H3 (PH3) expression vs. DNA content (DAPI) in Aspc1 cells treated with vehicle or PTC596 for 24 hours. **(E)** Percent of Aspc1 cells in mitosis ($PH3^+$/4N DNA content) after treatment for 24 hours with DMSO, PTC596, or 0.1μM nocodazole (NOC). **(F)** Representative histograms of DNA content measured by DAPI fluorescence in Aspc1 cells treated with vehicle or PTC596 at the indicated timepoints. **(G)** Percent of Aspc1 cells with DNA content >4N after treatment with DMSO or PTC596 at indicated timepoints. Two-way ANOVA, paired by experiment, with Dunnett's multiple comparisons test for treatment groups compared to control within each timepoint. **(H)** Representative flow cytometry scatter plots showing induction of apoptosis in Aspc1 cells following treatment with DMSO for 24 hours, or 1μM PTC596 at 24, 48, and 72 hours. Unfixed cells were stained for active caspase 3 and DAPI to distinguish viable cells (lower left) from early apoptosis (top left), late apoptosis (top right), and necrosis (lower right). **(I)** Total apoptotic Aspc1 cells (active caspase 3^+) were quantified for DMSO or PTC596 at each timepoint. Unless otherwise noted, statistical comparisons used a one-way ANOVA, paired by experiment, with Dunnett's correction for multiple comparisons for treatment groups compared to control. Error bars depict SEM over n= 3 biological replicates in each experiment. ***** $p< 0.05$, ****** $p< 0.005$, ******* $p<0.001$, ******** $p< 0.0001$.

Figure 2 – PTC596 has properties favorable for *in vivo* administration. (A) Plasma levels of PTC596 as measured by mass spectrometry at baseline, or 2, 4, 7, 24, or 48 hours following a single oral dose of PTC596 (10 mg/kg). Error = SD. n = 5 mice per time point. **(B)** Ratio of CC_{50} values for PTC596 treatment of MDCK-P-gp vs MDCK-WT cells. **(C)** Viability dose response curves of the indicated drugs for MDCK-WT (red) and MDCK-P-gp (blue) cells, alone (solid lines) or co-treated with the P-gp inhibitor Vasldopar (dashed lines). **(D)** Mass spectrometry measurements of PTC596 concentrations in tumor and normal tissues from six KPC, 24 hours following a single oral dose of PTC596 (17 mg/kg). **(E)** PTC596 concentrations in plasma, quadriceps, and PDA tissues from $KP^{f/f}C$ mice, 24 hour following a single oral dose of PTC596 (10mg/kg), alone or in combination with gemcitabine (100 mg/kg). **(F) Left -** Western blot for CYCLIN B1 on tumors from $KP^{fl/fl}C$ mice treated with 10 mg/kg PTC596 alone (n = 3). Tumor biopsy samples (Bx) were acquired by abdominal laparotomy 48 hours prior to first dose, and compared to samples acquired at necropsy (Nx) 24 hours after the third dose. **Right -** Quantification of CYCLIN B1 (CycB1) from the left panel, normalized to VINCULIN (Vinc). * $p < 0.05$ by paired t-test. **(G)** Body weights of KC mice treated for 30 days with PTC596 (q.w., p.o.) in combination with gemcitabine (100 mg/kg, b.i.w., i.p.). PTC596 was administered at 13 mg/kg, 15 mg/kg, or 17 mg/kg.

Figure 3– Combinatorial efficacy of PTC596 with gemcitabine in preclinical models of PDA. (A) nu/nu mice bearing Capan-1 xenograft tumors were treated with vehicle, PTC596 (12.5 mg/kg, b.i.w.), gemcitabine (40 mg/kg, b.i.w.), or PTC596 + gemcitabine for 45 days. Tumor volumes were measured twice per week. Bars = SD. N= 10 mice per treatment group. **(B)** Body weights from mice in (A) are plotted as percent original body weight. Bars = SD. **(C)** Body weights of KPC mice treated with 596/gem shows the regimen is well tolerated until mice succumb to disease. **(D)** Survival of KPC mice treated with vehicle (veh), gemcitabine (gem, 100mg/kg b.i.w.), PTC596 (596, 17mg/kg b.i.w.), or PTC596 + gemcitabine (596/gem). Median overall survival of the 596/gem arm was 33.5 days versus 11, 12.5, and 12.5 for the remaining arms). N= 10 mice/treatment arm. Significant pairwise comparisons indicated (log-rank test). **(E)** Tumor growth rate calculations calculated from longitudinal tumor volumes. Statistical comparisons show one-way ANOVA with Sidak's correction for the indicated pairs. **(F)** Quantification of IHC for phosphorylated Histone H3 (PH3) performed on KPC intervention study tumors following necropsy. Plots show average positive cells per 40X field over 10 fields per tumor. Bars= SEM. One-way ANOVA with Sidak's correction. **(G)** Quantification of IHC for cleaved Caspase-3 (CC3) performed on KPC intervention study tumors following necropsy. Plots show average positive cells per 40X field over 10 fields per tumor. Bars= SEM. One-way ANOVA with Sidak's correction. ***** $p < 0.05$, ****** $p < 0.005$, ******* $p < 0.001$, ******** $p < 0.0001$.

Figure 4 – The activity of PTC596 is independent of BMI1 in PDA cells. (A) Western blots showing BMI1 levels in Aspc1, MiaPaCa-2, and Panc1 cells treated for 24 hours with vehicle (VEH), 0.1 uM nocodazole (NOC), 0.1 uM 596 (0.1), or 1.0 uM 596 (1.0) relative to Vinculin (VINC) loading control. Both PTC596 and nocodazole induce accumulation of a lower mobility band. **(B)** Treatment of HT1080 protein lysates with λ phosphatase demonstrates that the lower mobility band induced by PTC596 is due to phosphorylation. **(C)** PCR showing *Bmi1* deletion in J1002 cells following treatment with tamoxifen. Upper band represents floxed allele. Lower band represents recombined allele after treatment. VEH= cells treated with 0.02% ethanol for 72 hours; TAM= cells treated with 5 uM tamoxifen for 72 hours; NEG= no DNA. POS= DNA from kidney tissue of a KPFBR mouse treated with tamoxifen. **(D)** Western blot showing loss of BMI1 protein expression in J1002TAM cells. **(E)** Relative viability of J1002VEH and J1002TAM cells treated with vehicle, 0.1 uM 596, or 1.0 uM 596 over 96 hours. Bars= SEM, N= 3 biological replicates, one-way ANOVA with Dunnett's correction comparing treatment groups to VEH. **(F)** Dose response curves for J1002VEH and J1002TAM cells treated with PTC596 for 72 hours. Viable cells quantified at endpoint by AlamarBlue. Bars= SEM, N= 3 biological replicates. **(G,H)** DNA content flow cytometry for J1002VEH cells (G) and J1002TAM cells (H). **Left** – Representative DNA histograms for cells treated for 24 hours with vehicle (VEH) or 1.0 uM PTC596. **Right** – Percent of cells in G0/G1 phase, S phase, G2/M phase for cells treated for 24 hours with vehicle (VEH) or 1.0 uM PTC596 (596). Bars= SEM, N= 3 biological replicates, t-test with Welch's correction. For all panels: ***** $p< 0.05$, ****** $p< 0.005$, ******* $p<0.001$, ******** $p< 0.0001$.

Figure 5 – PTC596 directly inhibits tubulin polymerization and synergizes with nab-paclitaxel *in vivo*. (A) Plot of differentially expressed genes measured by RNA-seq on ASPC1 cells treated with DMSO or 1μM PTC596, integrated over 8, 16, and 24 hour timepoints. Subsets of down-regulated (green) and up-regulated (orange) genes in cells treated with PTC596 are indicated. **(B)** Representative western blot from Aspc1 cells treated with vehicle (VEH), 3.0 uM PTC596 (596), 1.0 uM colchicine (COL), or 1.0 uM paclitaxel (TAX) for 2 hours. Following treatment, cell lysates were fractionated by centrifugation in order to separate free tubulin from microtubules. LSP = Low Speed Pellet (1,000 x g, 5 min), HSP = High Speed Pellet (100,000 x g, 1 hour), HSS = High Speed Supernatant (100,000 x g, 1 hour). **(C,D)** Representative immunofluorescence images of Aspc1 cells treated with vehicle (C) or PTC596 (D) for 24 hours. β-tubulin is shown in black and DAPI in blue. N= 3 biological replicates. Scale= 20 um. **(E)** Cell-free tubulin polymerization assay showing the ability of PTC596 to directly inhibit polymerization of free tubulin. **(F)** Maximal slope (fluorescence units/minute = polymerization rate) of three independent replicates of experiment in (E) shows that PTC596 significantly decreased the polymerization rate of tubulin, similar to colchicine (COL) and opposite of paclitaxel (TAX). Bars= SEM, one-way ANOVA with Dunnett's correction for treatment groups compared to VEH. ******* $p<0.001$, ******** $p< 0.0001$. **(G)** Average tumor volumes over time of subcutaneous patient-derived xenografts derived from a human PDA for the indicated treatment groups. Bars= SEM, N= 5 tumors per group. Selected two-way ANOVA comparisons indicated (ns= not significant, ******** $p< 0.0001$). **(H)** Percent of initial body weight over time for the mice from (G).

References

1. Raimondi S, Maisonneuve P, Lowenfels AB. Epidemiology of pancreatic cancer: an overview. Nat Rev Gastroenterol Hepatol 2009;6:699-708.

2. Siegel RL, Miller KD, Jemal A. Cancer statistics, 2019. CA Cancer J Clin 2019;69:7-34.

3. N H, AM N, M K, et al. SEER Cancer Statistics Review. https://seer.cancer.gov/csr/1975_2014/, 1975-2014.

4. Olive KP, Jacobetz MA, Davidson CJ, et al. Inhibition of Hedgehog signaling enhances delivery of chemotherapy in a mouse model of pancreatic cancer. Science 2009;324:1457-61.

5. Neesse A, Algul H, Tuveson DA, et al. Stromal biology and therapy in pancreatic cancer: a changing paradigm. Gut 2015;64:1476-84.

6. Hingorani SR, Petricoin EF, Maitra A, et al. Preinvasive and invasive ductal pancreatic cancer and its early detection in the mouse. Cancer Cell 2003;4:437-50.

7. Von Hoff DD, Ervin T, Arena FP, et al. Increased survival in pancreatic cancer with nab-paclitaxel plus gemcitabine. N Engl J Med 2013;369:1691-703.

8. Joerger M. Metabolism of the taxanes including nab-paclitaxel. Expert Opin Drug Metab Toxicol 2015;11:691-702.

9. Kim MJ, Cao L, Sheedy J, et al. Abstract 5517: PTC596-induced Bmi1 hyper-phosphorylation via Cdk1/2 activation resulting in tumor stem cell depletion, In AACR Annual Meeting, San Diego, CA, April 5-9, 2014, 2014.

10. Dobin A, Davis CA, Schlesinger F, et al. STAR: Ultrafast Universal RNA-Seq Aligner. Bioinformatics 2013;29:15-21.

11. Lawrence M, Huber W, Pages H, et al. Software for computing and annotating genomic ranges. PLoS Computational Biology 2013;9:e1003118.

12. Carlson M, Maintainer BP. TxDb.Hsapiens.UCSC.hg19.knownGene:Annotation Package for TxDb Object(s). 2015.

13. Ritchie ME, Phipson B, Wu D, et al. Limma powers differntial expression analyses for RNA-sequencing and microarray studies. Nucleic Acids Research 2015;43:e47.

14. Hanzelmann S, Castelo R, Guinney J. GSVA: gene set variation analysis for microarray and RNA-seq data. BMC Bioinformatics 2013;14:7.

15. Sastra SA, Olive KP. Quantification of murine pancreatic tumors by high-resolution ultrasound. Methods Mol Biol 2013;980:249-66.

16. Bednar FZ, Y. ; Nakada, D.; Simeone, D.M.; Morrison, S.J.; di Magliano, M.P. Bmi1 is required for murine pancreatic cancer initiatio. Pancreatic Cancer: Progress and Challenges. Lake Tahoe, NV, 2012.

17. Vleugel M, Hoogendoorn E, Snel B, et al. Evolution and function of the mitotic checkpoint. Dev Cell 2012;23:239-50.

18. Leonardo AD, Khan SH, Linke SP, et al. DNA Rereplication in the Presence of Mitotic Spindle Inhibitors in Human and Mouse Fibroblasts Lacking either p53 or pRb Function. Cancer Research 1997;57.

19. Xu WS, Perez G, Ngo L, et al. Induction of polyploidy by histone deacetylase inhibitor: a pathway for antitumor effects. Cancer Res 2005;65:7832-9.

20. Waddell N, Pajic M, Patch AM, et al. Whole genomes redefine the mutational landscape of pancreatic cancer. Nature 2015;518:495-501.

21. Nishida Y, Maeda A, Kim MJ, et al. The novel BMI-1 inhibitor PTC596 downregulates MCL-1 and induces p53-independent mitochondrial apoptosis in acute myeloid leukemia progenitor cells. Blood Cancer J 2017;7:e527.

22. Dey A, Xiong X, Crim A, et al. Evaluating the Mechanism and Therapeutic Potential of PTC-028, a Novel Inhibitor of BMI-1 Function in Ovarian Cancer. Mol Cancer Ther 2018;17:39-49.

23. Provenzano PP, Cuevas C, Chang AE, et al. Enzymatic targeting of the stroma ablates physical barriers to treatment of pancreatic ductal adenocarcinoma. Cancer Cell 2012;21:418-29.

24. Sastra SA, Olive KP. Acquisition of mouse tumor biopsies through abdominal laparotomy. Cold Spring Harb Protoc 2014;2014:47-56.

25. Wilkerson J, Abdallah K, Hugh-Jones C, et al. Estimation of tumour regression and growth rates during treatment in patients with advanced prostate cancer: a retrospective analysis. The Lancet Oncology 2017;18:143-154.

26. Jacobs JJL, Kieboom K, Marino S, et al. The oncogene and Polycomb group gene bmi-1 regulates cell proliferation and senescence through the ink4a locus. Nature 1999;397:164-168.

27. Song W, Tao K, Li H, et al. Bmi-1 is related to proliferation, survival and poor prognosis in pancreatic cancer. Cancer Sci 2010;101:1754-60.

28. Wu SQ, Niu WY, Li YP, et al. miR-203 inhibits cell growth and regulates G1/S transition by targeting Bmi-1 in myeloma cells. Mol Med Rep 2016;14:4795-4801.

29. Wang L, Liu JL, Yu L, et al. Downregulated miR-495 [Corrected] Inhibits the G1-S Phase Transition by Targeting Bmi-1 in Breast Cancer. Medicine (Baltimore) 2015;94:e718.

30. Zheng X, Wang Y, Liu B, et al. Bmi-1-shRNA inhibits the proliferation of lung adenocarcinoma cells by blocking the G1/S phase through decreasing cyclin D1 and increasing p21/p27 levels. Nucleic Acid Ther 2014;24:210-6.

31. Voncken JW, Schweizer D, Aagaard L, et al. Chromatin-association of the Polycomb group protein BMI1 is cell cycle-regulated and correlates with its phosphorylation status. Journal of Cell Science 1999;112:4627-4639.

32. Cleveland DW, Lopata MA, Sherline P, et al. Unpolymerized tubulin modulates the level of tubulin mRNAs. Cell 1981;25:537-546.

33. Goodson HV, Jonasson EM. Microtubules and Microtubule-Associated Proteins. Cold Spring Harb Perspect Biol 2018;10.

34. Spano JP, Bouillet T, Boaziz C, et al. Phase II study of paclitaxel combined with vinorelbine in patients with advanced breast cancer. Am J Clin Oncol 2004;27:317-21.

35. Costa G, Hreshchyshyn MM, Holland JF. Initial clinical studies with vincristine. Cancer Chemother Rep 1962;24:39-44.

36. Bates D, Eastman A. Microtubule destabilising agents: far more than just antimitotic anticancer drugs. Br J Clin Pharmacol 2017;83:255-268.

37. Jordan MA, Kamath K, Manna T, et al. The primary antimitotic mechanism of action of the synthetic halichondrin E7389 is suppression of microtubule growth. Mol Cancer Ther 2005;4:1086-95.

38. Seetharam M, Kolla KR, Chawla SP. Eribulin therapy for the treatment of patients with advanced soft tissue sarcoma. Future Oncol 2018;14:1531-1545.

39. Garland LL, Taylor C, Pilkington DL, et al. A phase I pharmacokinetic study of HMN-214, a novel oral stilbene derivative with polo-like kinase-1-interacting properties, in patients with advanced solid tumors. Clin Cancer Res 2006;12:5182-9.

40. LoRusso PM, Goncalves PH, Casetta L, et al. First-in-human phase 1 study of filanesib (ARRY-520), a kinesin spindle protein inhibitor, in patients with advanced solid tumors. Invest New Drugs 2015;33:440-9.

41. Cheung CH, Coumar MS, Hsieh HP, et al. Aurora kinase inhibitors in preclinical and clinical testing. Expert Opin. Investg Drugs 2009;18:379-398.

42. Komlodi-Pasztor E, Sackett DL, Fojo AT. Inhibitors targeting mitosis: tales of how great drugs against a promising target were brought down by a flawed rationale. Clin Cancer Res 2012;18:51-63.

43. Kulkarni RP, Castelino K, Majumdar A, et al. Intracellular transport dynamics of endosomes containing DNA polyplexes along the microtubule network. Biophys J 2006;90:L42-4.

44. Ganguly A, Yang H, Sharma R, et al. The role of microtubules and their dynamics in cell migration. J Biol Chem 2012;287:43359-69.

45. Giustiniani J, Daire V, Cantaloube I, et al. Tubulin acetylation favors Hsp90 recruitment to microtubules and stimulates the signaling function of the Hsp90 clients Akt/PKB and p53. Cell Signal 2009;21:529-39.

46. Schwartz EL. Antivascular actions of microtubule-binding drugs. Clin Cancer Res 2009;15:2594-601.

47. Kanthou C, Tozer GM. Microtubule depolymerizing vascular disrupting agents: novel therapeutic agents for oncology and other pathologies. Int J Exp Pathol 2009;90:284-94.

48. Infante JR, Bedard PL, Shapiro G, et al. Phase I results of PTC596, a novel small molecular targeting cancer stem cells (CSCs) by reducing levels of BMI1 protein. Journal of Clinical Oncology 2017;35:2574-2574.

49. Photiou A, Shah P, Leong LK, et al. In vitro Synergy of Paclitaxel (Taxol) and Vinorelbine (Navelbine) Against Human Melanoma Cell Lines. European Journal of Cancer 1997;33:463-470.

50. Giannakakou P, Villalba L, Li H, et al. Combinations of pacliataxel and vinblastine and their effects on tublin polymerization and cellular cytotoxicity: Characterization of a synergistic schedule. International Journal of Cancer 1998;75:57-63.

51. Knick VC, Eberwein DJ, Miller CG. Vinorelbine Tartrate and Paclitaxel Combinations-Enhanced Activity Against In Vivo P388 Murine Leukemia Cells. Journal of the National Cancer Institute 1995;87:1072-1077.

52. Martin M, Lluch A, Casado A, et al. Paclitaxel plus vinorelbine- An active regimen in metastatic breast cancer patients with prior anthracycline exposure. Annals of Oncology 2000;11:85-89.

53. Frese KK, Neesse A, Cook N, et al. nab-Paclitaxel potentiates gemcitabine activity by reducing cytidine deaminase levels in a mouse model of pancreatic cancer. Cancer Discov 2012;2:260-269.

54. Neesse A, Frese KK, Chan DS, et al. SPARC independent drug delivery and antitumour effects of nab-paclitaxel in genetically engineered mice. Gut 2014;63:974-83.

Author Manuscript Published OnlineFirst on June 7, 2019; DOI: 10.1158/1078-0432.CCR-18-3281
Author manuscripts have been peer reviewed and accepted for publication but have not yet been edited.

Figure 1

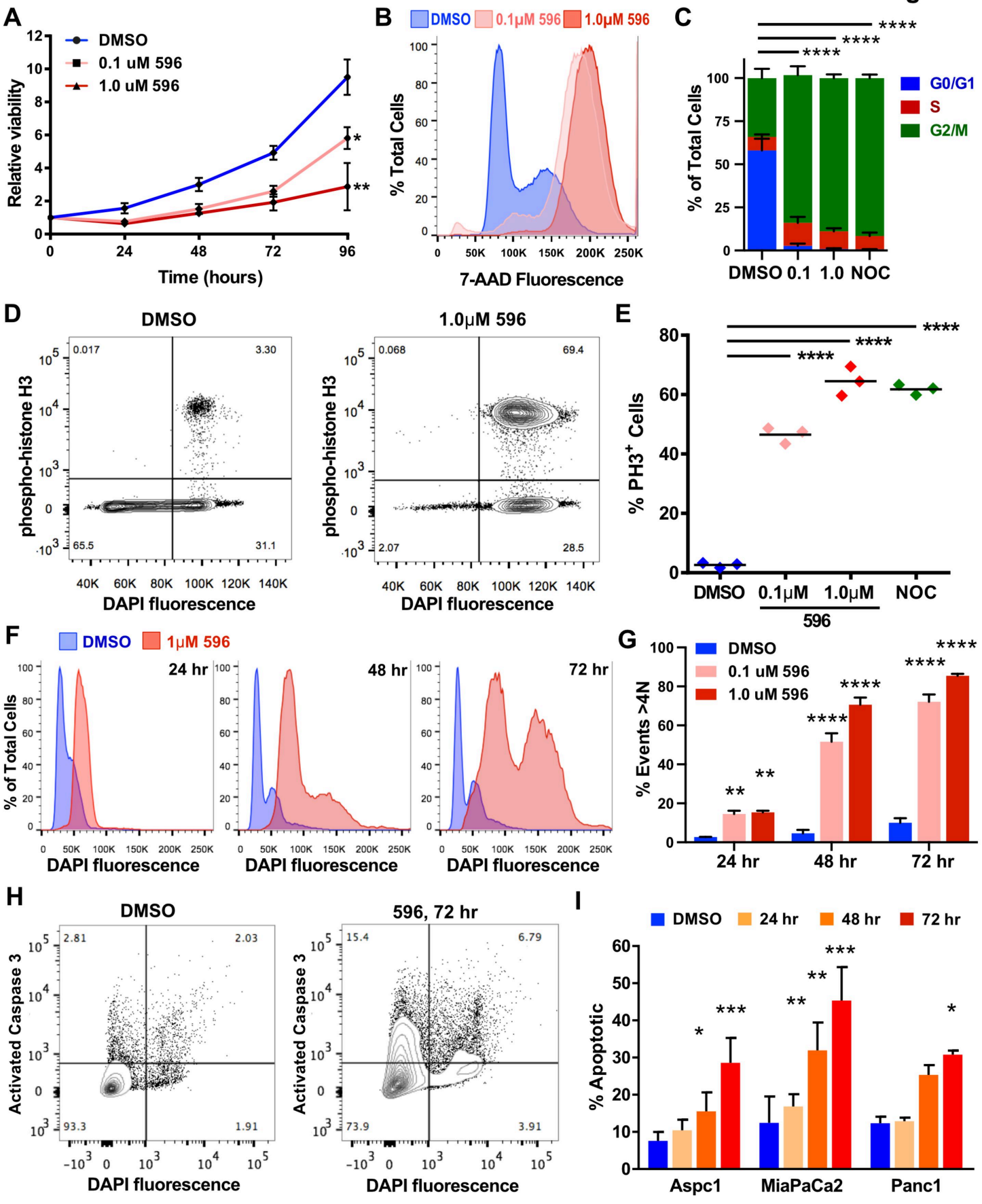

Author Manuscript Published OnlineFirst on June 7, 2019; DOI: 10.1158/1078-0432.CCR-18-3281
Author manuscripts have been peer reviewed and accepted for publication but have not yet been edited.

Figure 2

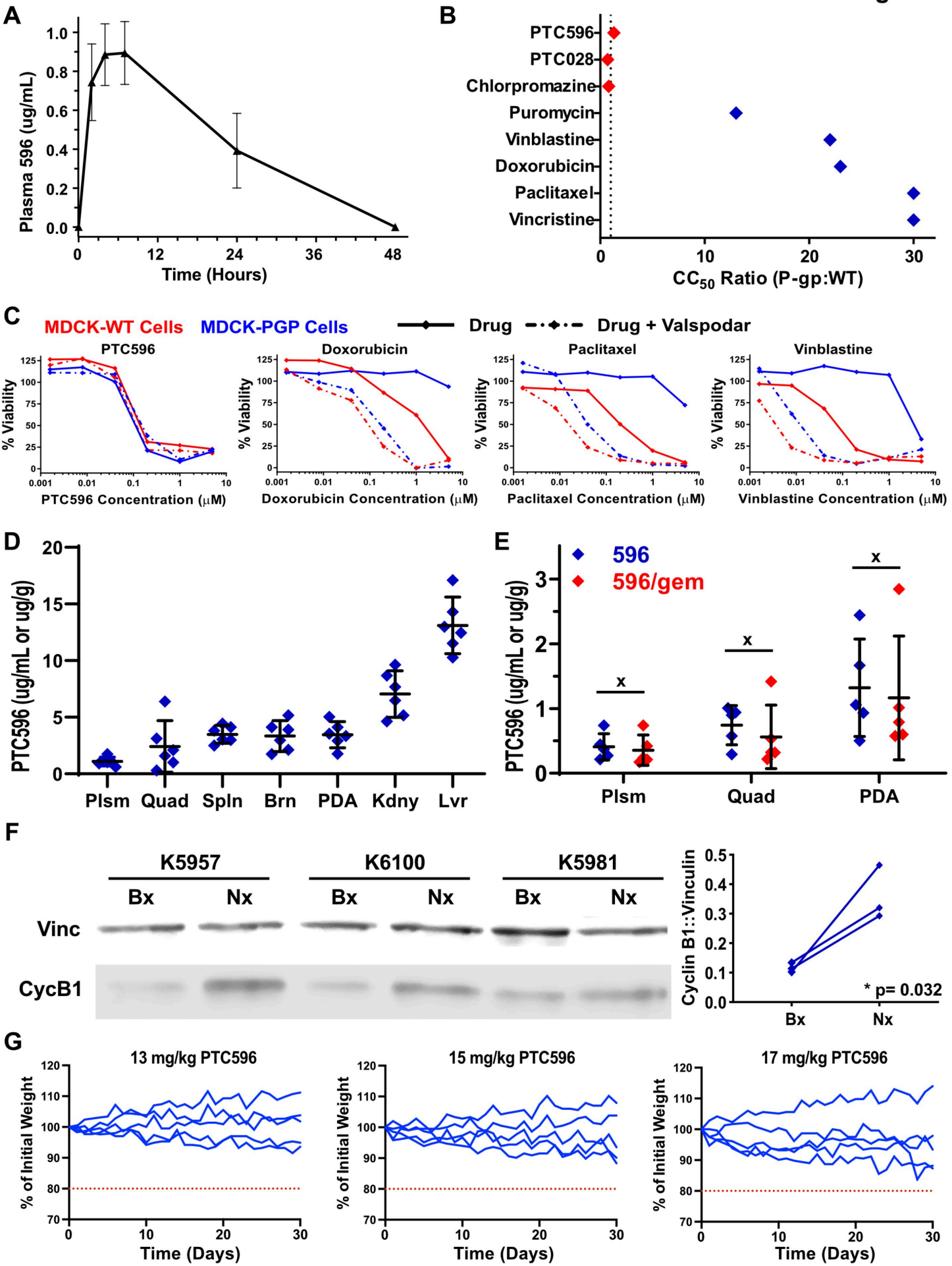

Author Manuscript Published OnlineFirst on June 7, 2019; DOI: 10.1158/1078-0432.CCR-18-3281
Author manuscripts have been peer reviewed and accepted for publication but have not yet been edited.

Figure 3

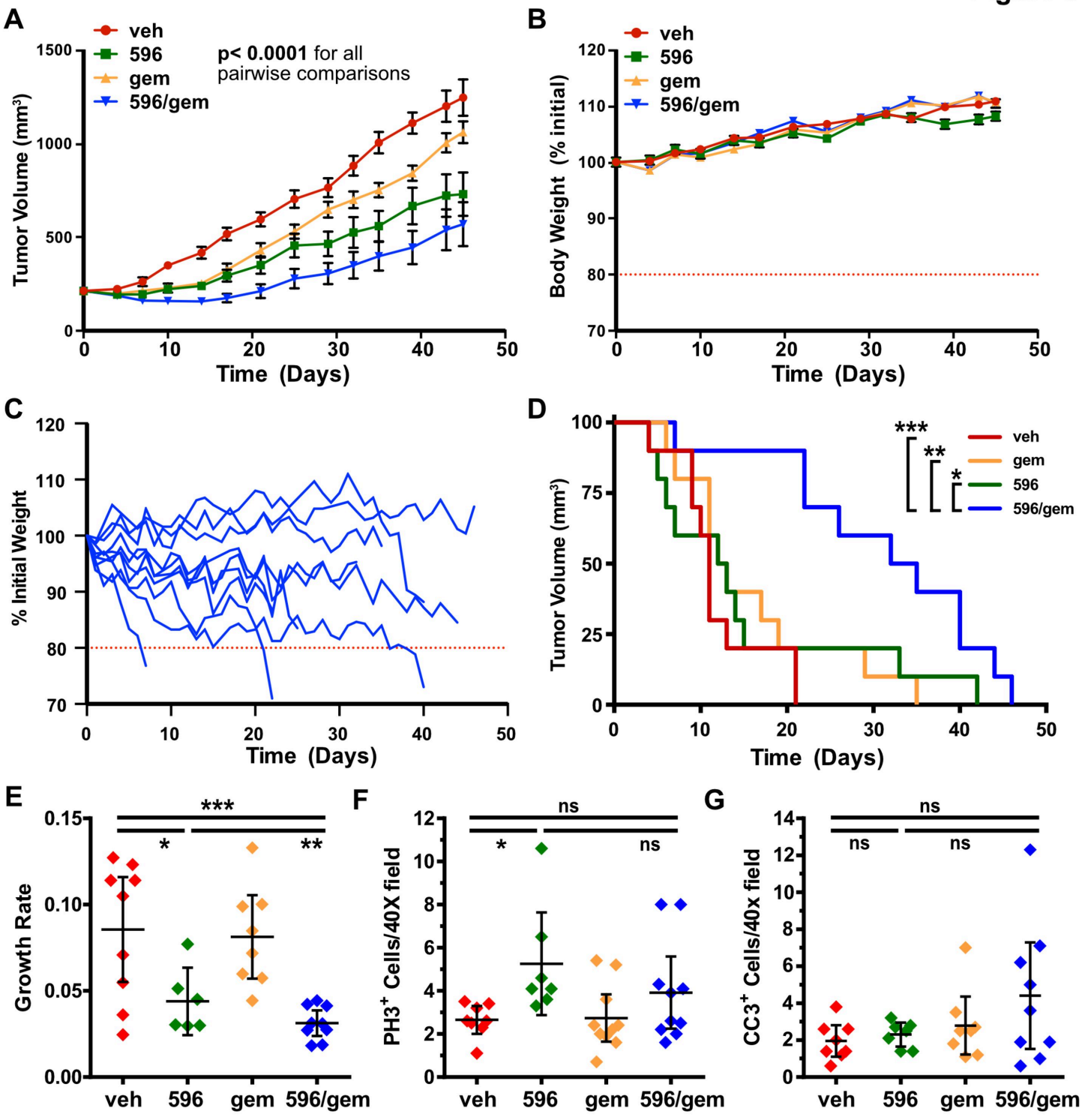

Author Manuscript Published OnlineFirst on June 7, 2019; DOI: 10.1158/1078-0432.CCR-18-3281
Author manuscripts have been peer reviewed and accepted for publication but have not yet been edited.

Figure 4

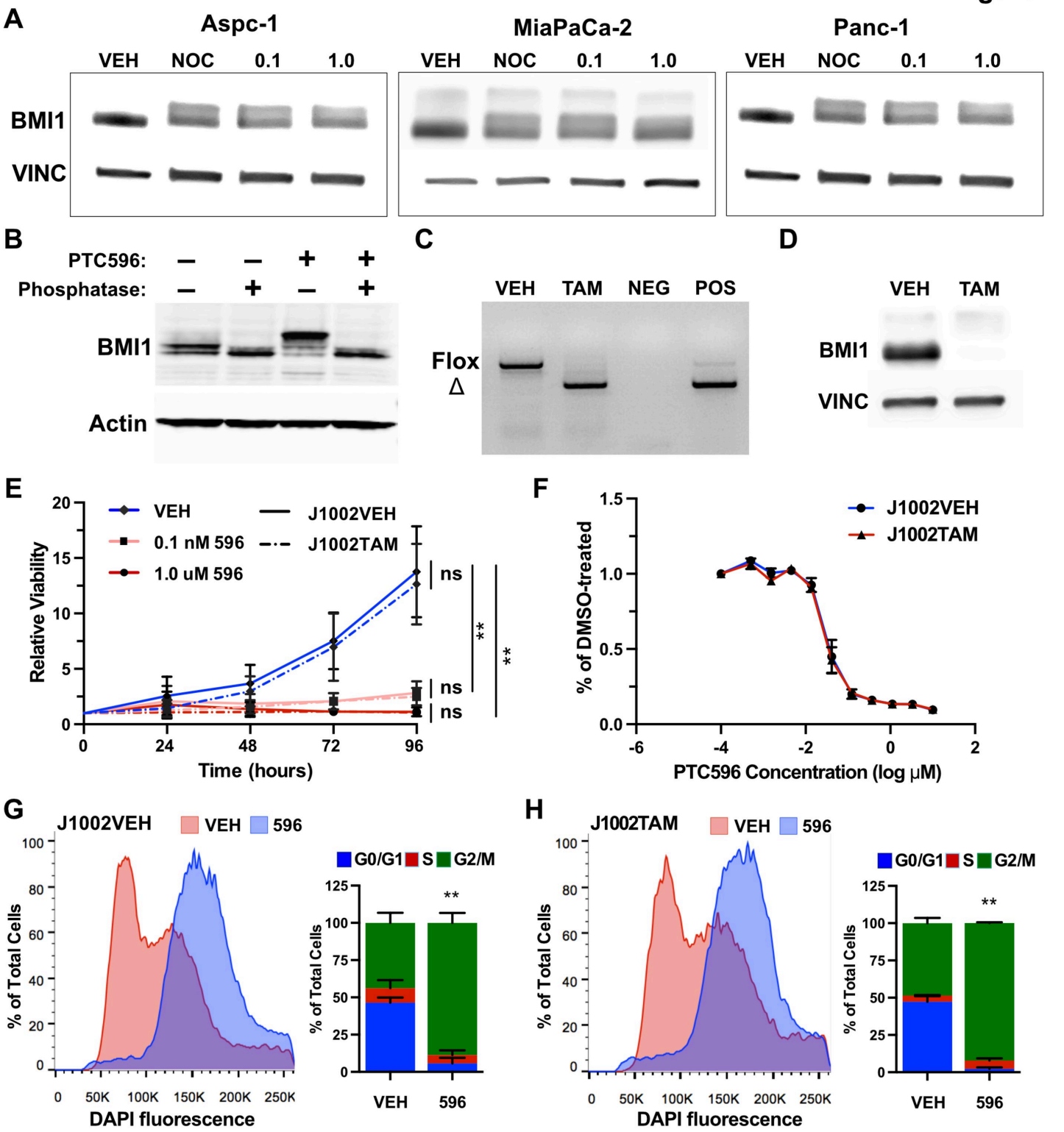

Author Manuscript Published OnlineFirst on June 7, 2019; DOI: 10.1158/1078-0432.CCR-18-3281
Author manuscripts have been peer reviewed and accepted for publication but have not yet been edited.

Figure 5

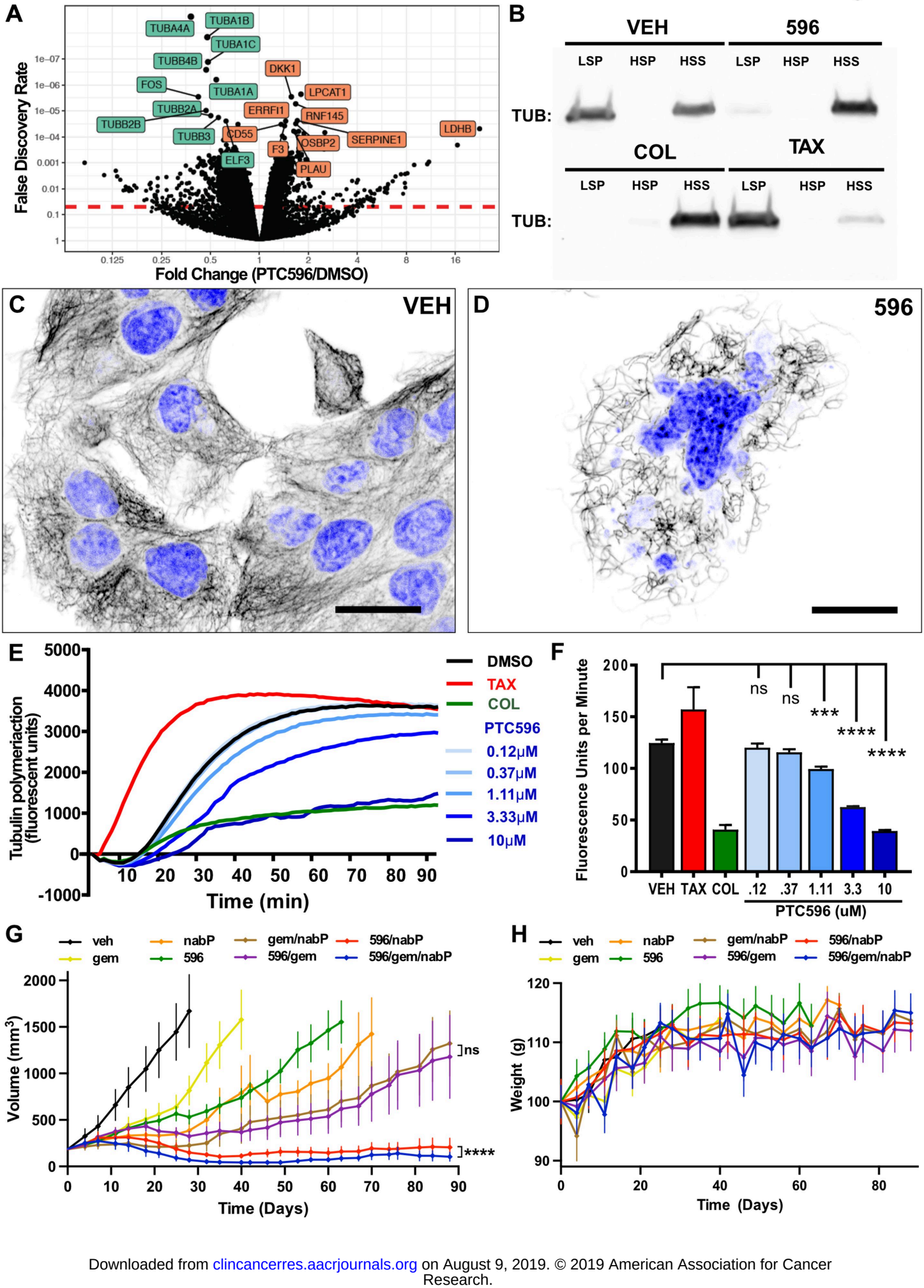

AACR American Association for Cancer Research

Clinical Cancer Research

Effective delivery of a microtubule polymerization inhibitor synergizes with standard regimens in models of pancreatic ductal adenocarcinoma

Jaime A Eberle-Singh, Irina Sagalovskiy, H. Carlo Maurer, et al.

Clin Cancer Res Published OnlineFirst June 7, 2019.